

NASA Technical Memorandum 103111

# Computational Modeling and Validation for Hypersonic Inlets

Louis A. Povinelli  
*Lewis Research Center*  
*Cleveland, Ohio*

(NASA-TM-103111) COMPUTATIONAL MODELING AND  
VALIDATION FOR HYPERSONIC INLETS (NASA)  
11 D CSCL 20D

N90-22011

Unclass

G3/34 0280100

Prepared for the  
75th Symposium on Hypersonic Combined Cycle Propulsion  
sponsored by the Propulsion and Energetics Panel of AGARD  
Madrid, Spain, May 28—June 1, 1990

**NASA**



# COMPUTATIONAL MODELING AND VALIDATION FOR HYPERSONIC INLETS

Louis A. Povinelli  
National Aeronautics and Space Administration  
Lewis Research Center  
21000 Brookpark Road  
Cleveland, Ohio 44135 U.S.A.

## SUMMARY

Hypersonic inlet research activity at NASA is reviewed. The basis for the paper is the experimental tests performed with three inlets: the NASA Lewis Research Center Mach 5, the McDonnell Douglas Mach 12, and the NASA Langley Mach 18. Both three-dimensional PNS and NS codes have been used to compute the flow within the three inlets. Modeling assumptions in the codes involve the turbulence model, the nature of the boundary layer, shock wave-boundary layer interaction, and the flow spilled to the outside of the inlet. Use of the codes in conjunction with the experimental data are helping to develop a clearer understanding of the inlet flow physics and to focus on the modeling improvements required in order to arrive at validated codes.

## INTRODUCTION

This paper presents a review of the hypersonic inlet activities at NASA. Generally, the NASA work has covered the range from Mach 5 to 18. The research has been of a computational and experimental nature with a two-fold objective: (1) to develop an improved understanding of the physics and chemistry of inlet flow fields and (2) to validate the numerical codes used for high-speed inlets. The objectives result from the basic philosophy developed for the National Aerospace Plane project; namely, that numerical codes can be validated using ground test data and extrapolated to higher velocities. Since the ground experimental data base is limited to Mach 8 and lower, extrapolation of the computational methods must be made from Mach 8 to the Mach number, approximately 16, where airbreathing propulsion terminates.

A number of codes have been used to date within NASA for inlet flows. Code development and modifications have taken place over the last several years and the emphasis today is on the application to various inlets that have been tested. Those inlets include the Mach 5 inlet at NASA Lewis Research Center, a General Dynamics Mach 12 configuration and a Mach 18 NASA Langley inlet. Only a limited amount of data is available for each configuration.

The numerical methods used have included a PNS code, the PARC NS code, the SCRAM3D and CFL3D. Generally, the codes employ a Baldwin-Lomax turbulence model. Assumptions are made regarding the state of the boundary layer and spillage has generally not been computed. Thick upstream boundary layers are computed in some cases having a forward extension surface. In this paper a comparison of the experimental and computational results will be reviewed.

## RESULTS

### Mach 12 Generic Inlet

The simple rectangular inlet configuration shown in Fig. 1 was tested at Mach 12.26. A flat plate of 30-in. length preceded the entrance to the inlet in order to simulate the boundary layer growth on the forebody of a hypersonic aircraft. Compression wedges form the top and bottom walls of the inlet and the contraction ratio was equal to 5. Swept sidewalls which connect the upper and lower walls prevent compressed flow from spilling over the inlet sides.

Computations were made with a three-dimensional PNS LBI implicit scheme (Ref. 1) with grids of 80 by 60 by 750 on a Cray X-MP. This solver includes real gas effects (Ref. 2) as well as dissociation and ionization modeling (Ref. 3). For this experiment, however, the inlet air was only heated sufficiently to avoid condensation, and the real gas modeling was not required. The issues that are of importance in this computation are the assumptions regarding the state of the boundary layer, the turbulence model, spillage of flow around the sideplates and shock boundary layer interaction. For the PNS computation it was assumed that the boundary layer was turbulent starting on the leading edge of the flat plate, the cowl leading edge and the sidewall leading edges. The turbulence model used was a Baldwin-Lomax model and spillage was not considered. Modeling of the shock boundary layer interaction involved the use of a flare approximation in order to allow the PNS to march through the region of flow separation. The results of the PNS solution are shown in Fig. 2. Contour plots of constant Mach number within the inlet are shown. The concentration of lines near the walls indicate the boundary layers, while concentrated contours in the freestream indicate shock wave locations. The flow features seen are boundary layer buildup on the flat plate followed by thickening on the sidewalls and ramp surface. Shocks generated by the compression wedges are seen as horizontal lines, and the sidewall shocks are vertical lines.

Basically, the important physics occurring are that the low energy flow in the sidewall boundary layer has been swept up the sidewall by the ramp shock, and then down the sidewall by the cowl shock. Further downstream, the shock waves cross and are distorted by interaction with the sidewall boundary layers and the expansion fan on the ramp surface. Additional complex interactions then occur as the flow moves downstream. The PNS solution fails when the ramp shock wave reflects from the cowl and strikes the ramp surface, resulting in large corner separation of the low energy flow.

An alternate view of the three-dimensional flow is obtained with sidewall particle tracing (Fig. 4). Interaction of the ramp and cowl shocks with the sidewall boundary layer causes the particles to converge near the shock interaction point. The particles are then displaced due to the vortex motion. Flow migration details are evident in this computational simulation. As a sidenote, since the vortex persists downstream, it has been proposed that enhanced fuel mixing could occur with judicious injector locations downstream (Ref. 4).

Navier-Stokes computations have also been carried out for the generic inlet at NASA Langley with CFL3D (Ref. 5). In this case, the boundary layers were assumed turbulent on all surfaces from the leading edges. The turbulence model used was a Baldwin-Lomax model and spillage over the sideplates was not considered. In the vicinity of the shock boundary no special modeling was employed. Figure 5(a) shows the pressure distributions for the ramp and centerline cowl surfaces. Figure 5(b) shows the side plane distributions. Comparison of the CFL3D results and the experimental data show good agreement, particularly along the centerline where shock locations appear to be well resolved by the code. The viscous interactions occurring along the side plane are not accurately resolved. There is a significant underprediction of the pressure on the ramp side (Fig. 5(b)). In addition, CFL3D was used to compute the heat transfer on the ramp and cowl surfaces (Figs. 6(a) and (b)). The experimental peak heat fluxes are underpredicted for the ramp centerline but well predicted for the cowl surface.

For the ramp and cowl side planes (Fig. 6(b)), the peak prediction is lower on the ramp whereas the cowl side prediction is not qualitatively correct. Again, strong viscous effects are predominating along the side walls of the inlet in agreement with the complex behavior shown in Figs. 2 to 4. Further analysis of the Mach 12 inlet is underway at the NASA Centers and industry.

#### Mach 5 Inlet

A rectangular mixed compression inlet designed for Mach 5 operation and tested at NASA Lewis is shown in Figs. 7(a) and (b) (Ref. 6). A series of ramps generate oblique shock waves external to the cowl. An oblique shock from the cowl leading edge reflects from the ramp surface and terminates in a normal shock downstream of the inlet throat. Operation in the wind tunnel was such that a Mach number of 4.1 occurred on the first ramp. The inlet incorporates variable geometry with collapsible ramp and variable bleed exits on the cowl, sidewalls and ramps. Bleed of 0.5 percent was removed on the ramp upstream of the shoulder. Additional bleed from the cowl and sidewalls was approximately 8.8 percent of the capture mass flow. Figure 8 shows the location of pressure rakes and probes in the model. A 0.5-in. strip of grit was applied near the leading edges of the ramp and sidewall to ensure that a fully turbulent boundary layer was ingested by the inlet.

Navier-Stokes computations were carried out using the PARC3D solver (Ref. 7) on the NAS Cray 2. Grid sizes of 151 by 81 by 41 were used with hyperbolic packing so that the first point was at a  $y^+$  of 2. Bleed was simulated by imposing a constant mass flux through the porous bleed surfaces based on the experimental data. The boundary layer was assumed to be turbulent throughout, and the turbulence model was that of Baldwin-Lomax. Flow spillage over the sideplates was also not computed in this case.

The computed ramp pressure results are compared with experimental data in Fig. 9. The agreement of the computations with the data is very good throughout the computed length of the inlet. Figure 10 shows the comparison for the cowl pressure distribution. The disagreement of the results at an  $x/h$  of 4.2 is believed to be due to the fact that one of the translating probe assemblies is located in the same region where the four static pressure taps are located. Because the retracting probe does not completely retract into the wall, additional shocks are generated which biased the data. Pitot pressure profiles were compared with data at various locations along the inlet. Figure 11 shows the pressure profile from rake 3 which was located on the centerline and in the region of the second ramp (Fig. 8). The agreement of data and computation is very good. Along the sidewall, however, the agreement is much poorer, as shown in Fig. 12 for rake 7. The corner effects are not being adequately simulated. An improved turbulence model may improve the comparison in these corner regions. Figure 13 shows the pitot pressure comparison for rake 10 mounted at  $45^\circ$  from the corner of the cowl and sidewall at station 59.6 from the start of the inlet. This region of the flow is dominated by low energy vortical flow as seen in Fig. 14. Large variations in the pitot pressure are seen as one moves from the corner into the stream. Measurements in these regions are also very difficult.

The Mach 5 inlet was also analyzed using the SCRAM3D Navier-Stokes code by Rose (Ref. 8). A Baldwin-Lomax turbulence was used, assuming turbulent boundary layers. These results also reveal strong glancing shock wave-boundary layer interaction leading to large regions of low momentum flow on the sidewalls. Rose carried out a number of numerical experiments to control the vortex phenomena in the corner regions. Figure 16

shows the baseline or no control case, followed by cowl cutback, cowl bleed and removal of a part of the sidewall. These modifications were made near the inlet ramp shoulder. It may be seen that these modifications were ineffective in eliminating the vortex region. Even with the cutback sidewall, the low momentum fluid exists along the entire sidewall. Some attenuation is seen along the cowl surface for that case. It is evident, however, that the shock-boundary layer physics within a rectangular shaped inlet will lead to pressure losses in the corner regions. However, if these regions can be utilized in an "integrated design approach" (Ref. 4), then combustor/nozzle design may benefit substantially. Further computations of the Mach 5 inlet with improved simulation of the bleed zones is underway, as well as further analysis of the test data.

#### Mach 18 Sidewall Compression Inlet

A sidewall compression inlet has been designed and tested at NASA Langley by Trexler. As seen in Fig. 17, the compression occurs on the sideplates. The experiments were run at an entrance Mach number of 18 to 22 with and without a flat plate upstream to simulate fuselage boundary layer buildup. The entering boundary layer was approximately one-third the cowl height. Computations were made by Rose (Ref. 9) using the SCRAM3D code. Laminar boundary layers were assumed on cowl and sidewalls, and a Baldwin-Lomax turbulence model was used.

Figure 18 shows the Mach number contours along the vertical centerplane for an entrance Mach number of 18.1. The contraction ratio was 4 and the cowl leading edge is located at the entrance to the constant area section. All of the convergence occurs along the sidewalls, which generate a pair of shock waves that intersect on the vertical centerplane. A large pressure rise is felt on the ramp surface. Further downstream, the shocks interact with the sidewall boundary layers and reflect and intersect again on the centerplane at the indicated position. A further rise in pressure causes ramp boundary layer separation.

The Mach number contours on the horizontal centerplane are shown in Fig. 19. The intersecting sidewall shocks and the intersecting reflected shocks are visible. Since the sidewall shocks strike the sidewall well upstream of the shoulder, shock cancellation is clearly not achieved. The reflected shock waves, however, are seen to cancel at the shoulder. The strong viscous interaction effects are very evident at these flow conditions.

Calculated Mach number contours are shown in Fig. 20 for both the horizontal and the vertical center planes with an entrance boundary layer. The entrance plate reduces the Mach number from the entrance value to about Mach 12. Separation of the boundary layer on the ramp, caused by the sidewall shock waves, causes a large upstream influence. As the ramp boundary layer thickens, an oblique shock occurs reducing the inlet flow to Mach 8. Sidewall shocks and their intersection are seen in the horizontal centerplane. The sidewall shock wave angle is substantially increased due to the reduced Mach number entering the inlet. The ramp shock falls outside the cowl leading edge. Figure 21 shows a comparison of the experimental and computed surface pressure distributions on the ramp centerline, for the case where the cowl is moved forward. In this particular comparison, the numerical code yields results which are higher than the measured data and also rises faster than measured. Further data analysis and comparisons are underway at the present time, which will lead to a more complete understanding of the flow in this class of inlets.

#### CONCLUSIONS

Through the use of a variety of numerical simulations and experiments, the basic flow features within rectangular hypersonic inlets are becoming better understood. Fast running PNS solvers in combination with much longer running but more sophisticated Navier-Stokes codes are providing a clearer picture of shock structure and boundary layer behavior in inlets. Clearly, the flow fields are highly three-dimensional, viscously dominated and contain significant flow separations. Shock wave-boundary layer interactions persist down to the throat and beyond. As the propulsion community moves towards the validation of these codes, a number of issues still remain which will impede the application of the methods for the design of hypersonic inlets. Perhaps the first concern is that regarding the nature of the boundary layer within the inlet. Although attempts are made to ensure the presence of turbulent layers, for example, questions still remain regarding the existence of transitional layers. Installation of hot film gauges on the walls would provide the numerical analyst with the proper information to use within his computer code; be it laminar, transitional or turbulent. An additional issue is concerned with turbulence modeling and the ability of the Baldwin-Lomax model in regions of glancing shock wave-boundary layer interaction. Current turbulence models appear to yield good qualitative flow characteristics, but may be inadequate for quantitative predictions. Alternate models are needed. A third concern deals with the necessity of including the zone outside of the inlet in order to provide proper boundary conditions for the computation. In spite of these concerns, the understanding and agreement (i.e., on centerline) are very significant. The Mach 5 inlet presents the same concerns but with the complication of bleed flow on all four surfaces. Modeling issues related to turbulence, boundary layer transition and spillage are made more complex with a distributed mass flux boundary condition. Again, it is remarkable that such good agreement, with limited data, was achieved for that inlet. A great deal more effort will be required to analyze the test data and develop the proper modeling for a bulk of the data.

The sidewall compression presents a unique approach to inlet design. Computations of the three-dimensional flow field and associated shock structure provide us with a great deal of physics. The limited data provides a basis for an improvement in current modeling. Use of the experimental data and empirically derived correlations may serve as a basis to produce improved viscous modeling. It is important to point out that in all of these inlet tests, the tunnel flow was sufficiently low to avoid real gas effects. Hence, the comparisons presented in the paper are only aerodynamic in nature. More significant modeling issues will surface as test data is acquired in high-enthalpy flows. Finally, the need to analyze variable geometry with transient disturbances will provide a significant challenge.

#### REFERENCES

1. Reddy, D.R., Smith, G.E., Liou, M.-F., and Benson, T.J., "Three Dimensional Viscous Analysis of a Hypersonic Inlet," AIAA Paper 89-0004, Jan. 1989. (Also, NASA TM-101474, 1989.)
2. Liou, M.-F., "Three Dimensional PNS Solutions of Hypersonic Internal Flows With Equilibrium Chemistry," AIAA Paper 89-0002, Jan. 1989.
3. Yu, S.-T., McBride, B.J., Hsieh, K.-C., and Shuen, J.-S., "Numerical Simulation of Hypersonic Inlet Flows with Equilibrium or Finite Rate Chemistry," AIAA Paper 88-0273, Jan. 1988.
4. Povinelli, L.A., "Advanced Computational Techniques for Hypersonic Propulsion," NASA TM-102005, 1989. Presented at the Ninth International Symposium on Air Breathing Engines, Athens, Greece, Sept. 4-9, 1989.
5. Diley, A., Eppard, W., and Switzer, G., "Zonal Analysis of Two High Speed Inlets," Presented at the CFD Symposium on Aeropropulsion, NASA Lewis Research Center, Cleveland, OH, April 24-26, 1990.
6. Weir, L.J., Reddy, D.R., and Rupp, G.D., "Mach 5 Inlet CFD and Experimental Results," AIAA Paper 89-2355, July 1989.
7. Reddy, D.R., Benson, T.J., and Weir, L.J., "Comparison of 3-D Viscous Flow Computations of Mach 5 Inlet with Experimental Data," AIAA Paper 90-0600, Jan. 1990.
8. Rose, W.C., and Perkins, E.W., "Innovative Boundary Layer Control Methods in High Speed Inlet Systems-Final Report," Contract NAS3-25408, Sept. 9, 1988 (NASA CR in publication).
9. Rose, W.C., Perkins, E.W., and Benze, D.P., NASA Ames Research Review, Dec. 1989.

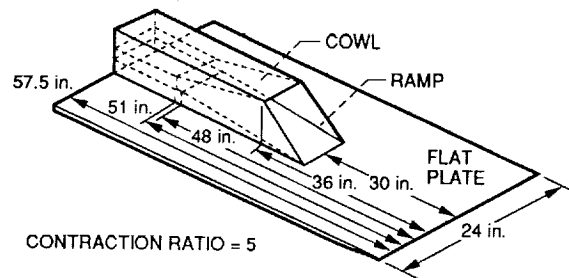


Figure 1. - Generic inlet (ref. 5).

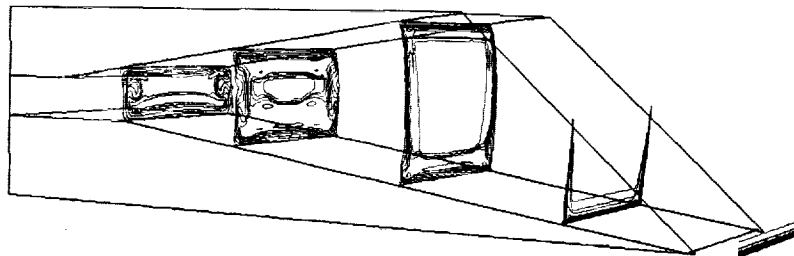


Figure 2. - Mach number contours,  $M = 12.25$  (ref. 1).

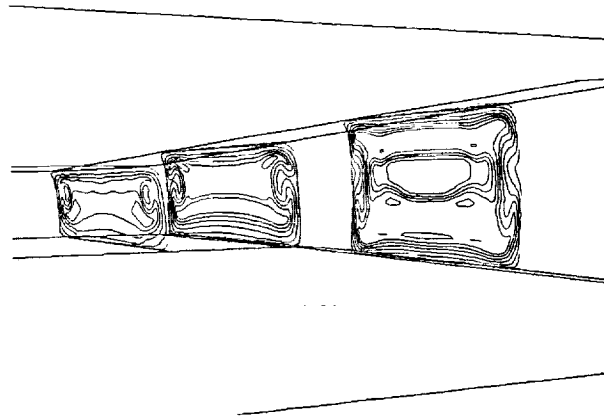


Figure 3. - Mach number contours viewed from aft (ref. 1).

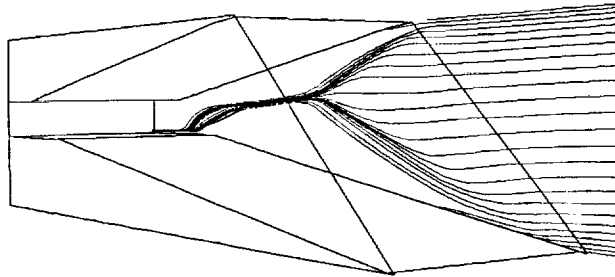


Figure 4. - Sidewall particle tracing,  $M = 12.25$  (ref. 1).

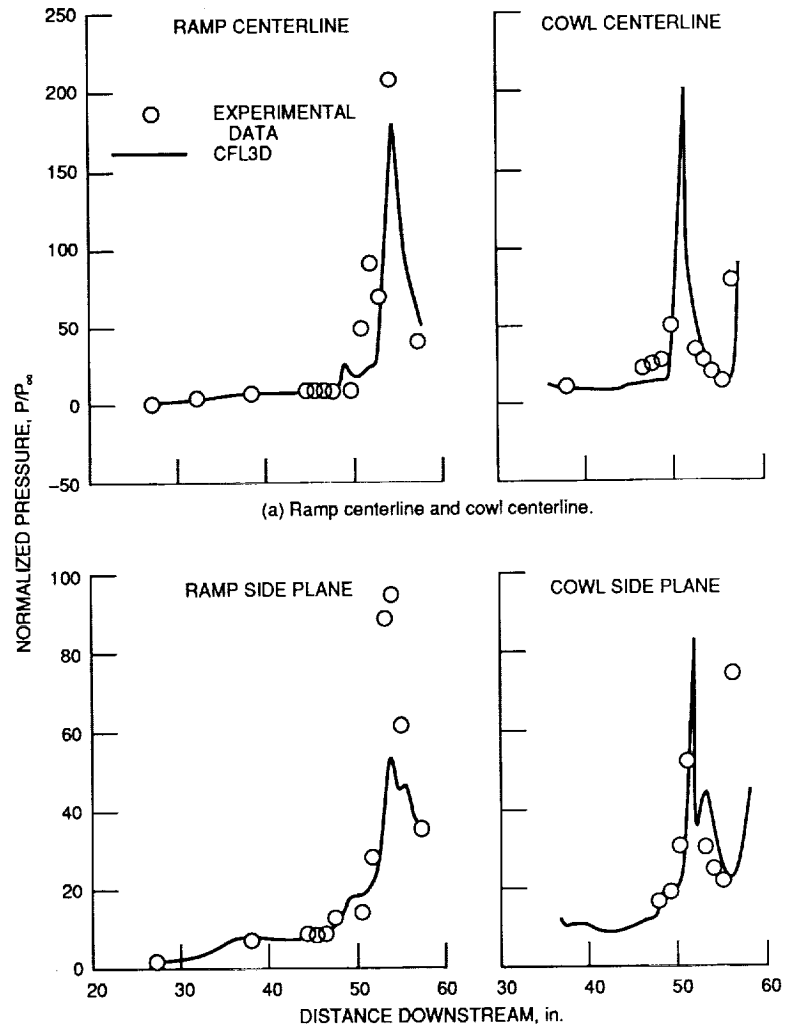
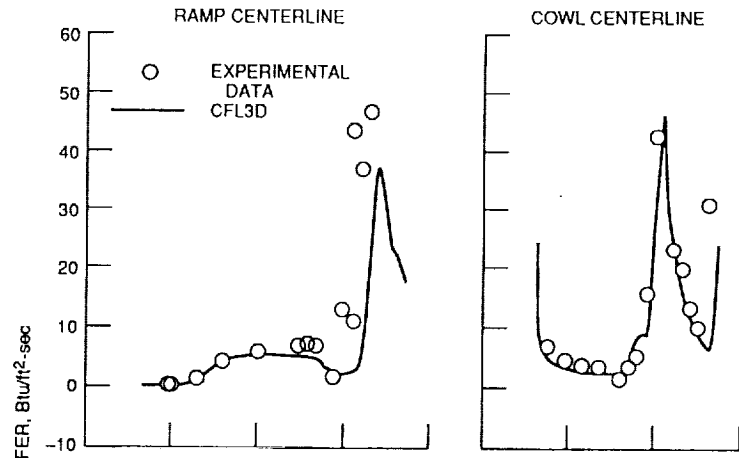
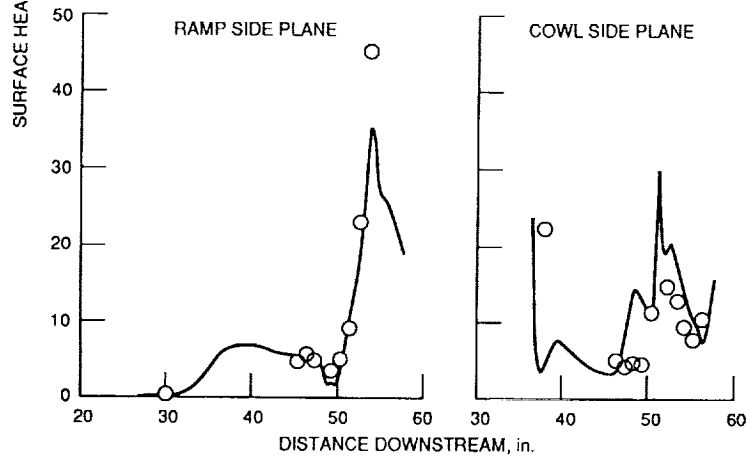


Figure 5. - Pressure comparisons (ref. 5).

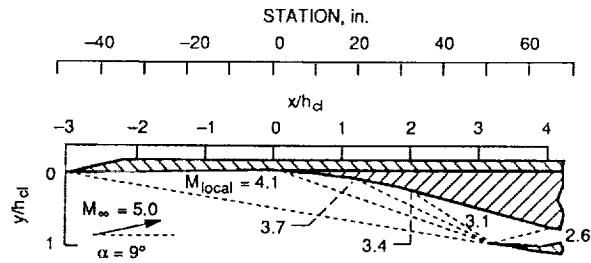


(a) Ramp centerline and cowl centerline.

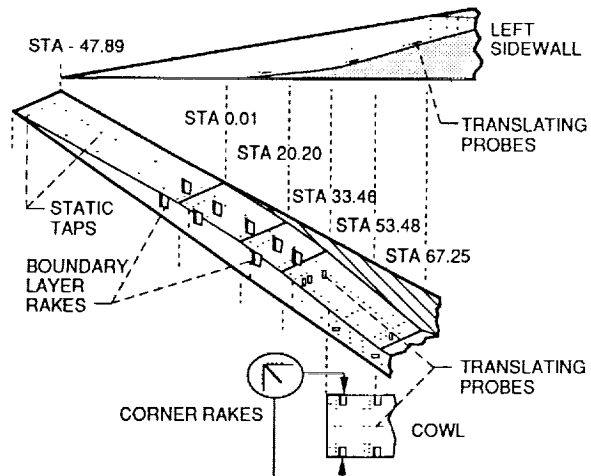


(b) Ramp side plane and cowl side plane.

Figure 6. - Heat transfer comparisons (ref. 5).



(a) Inlet compression system to ramp shoulder.



(b) Instrumentation upstream of inlet shoulder.

Figure 7. - (ref. 6).

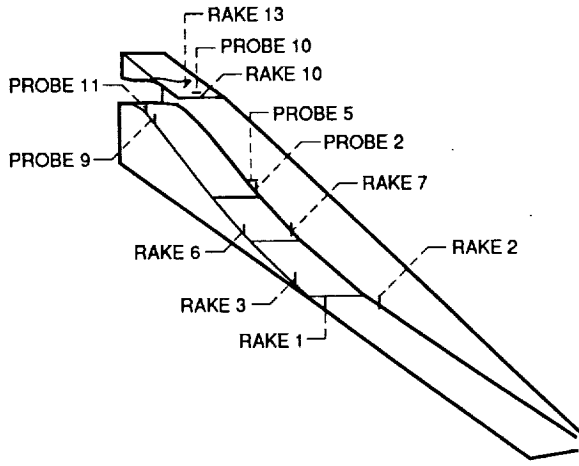


Figure 8. - Location of fixed rakes and translating probes used for pitot pressure measurement (ref. 7).

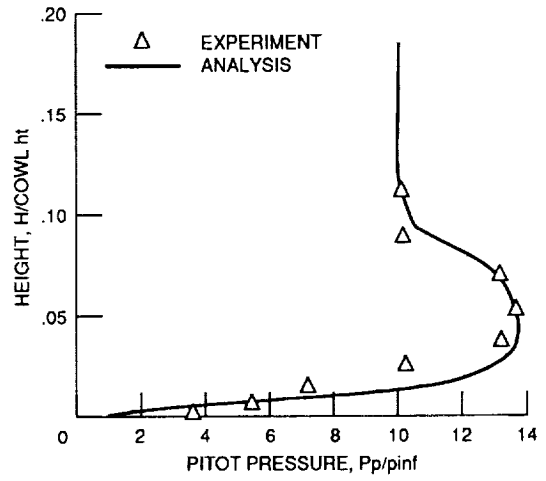


Figure 11. - Rake 3 pitot pressure profile (ref. 7).

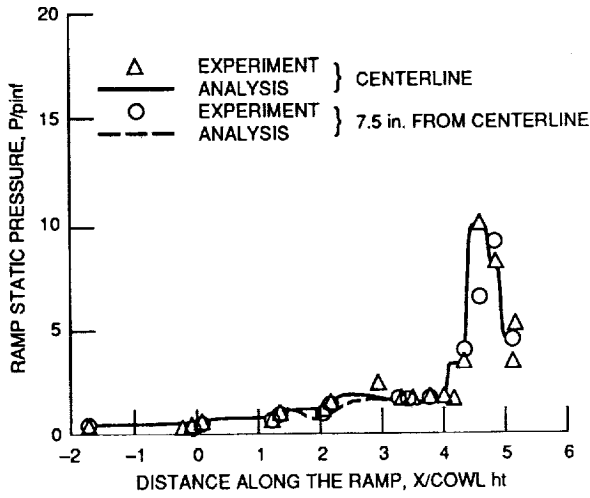


Figure 9. - Ramp static pressure distribution (ref. 7).

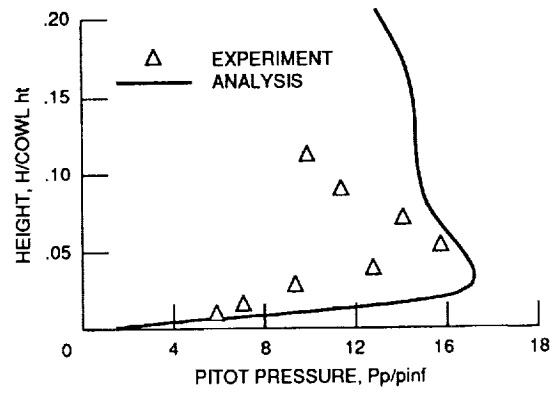


Figure 12. - Rake 7 pitot pressure profile (ref. 7).

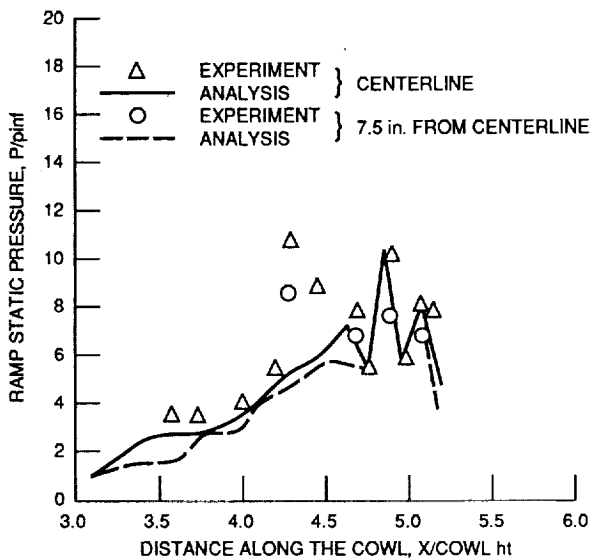


Figure 10. - Cowl static pressure distribution (ref. 7).

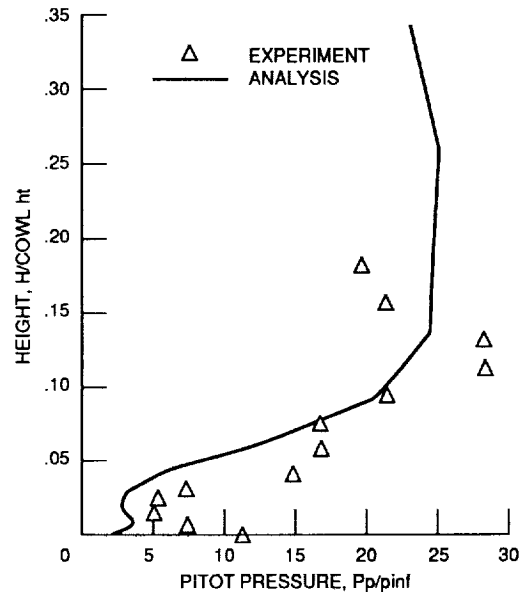


Figure 13. - Rake 10 pitot pressure profile (ref. 7).

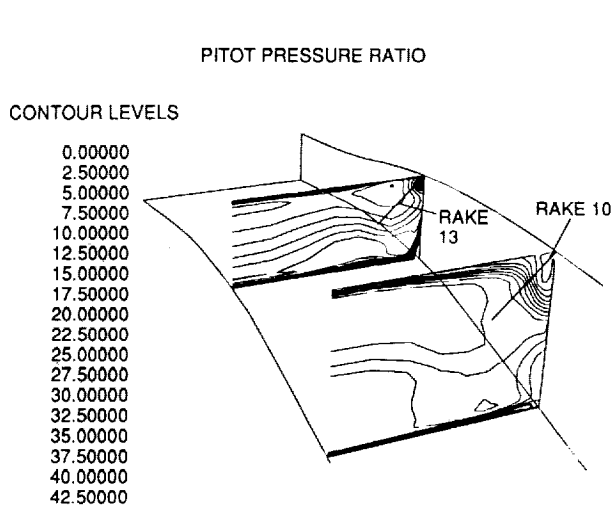


FIGURE 14. - Pitot pressure contour at rake 10 and rake 13 (ref. 7).

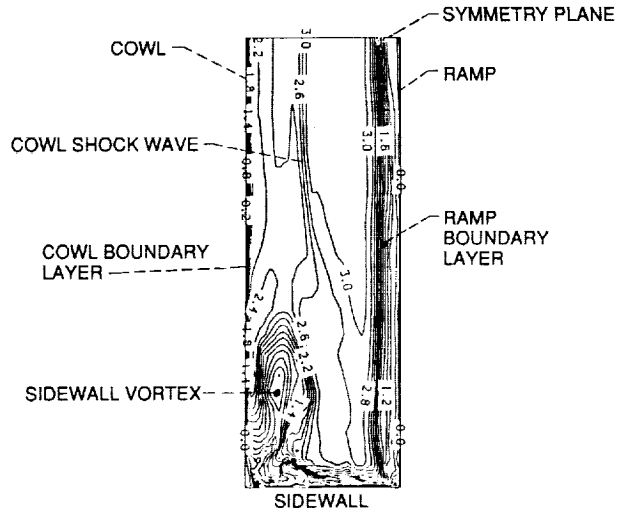


Figure 15. - Orientation of crossflow plane 150 located near the ramp shoulder showing plane of symmetry, sidewall ramp and cowl surfaces (ref. 8).

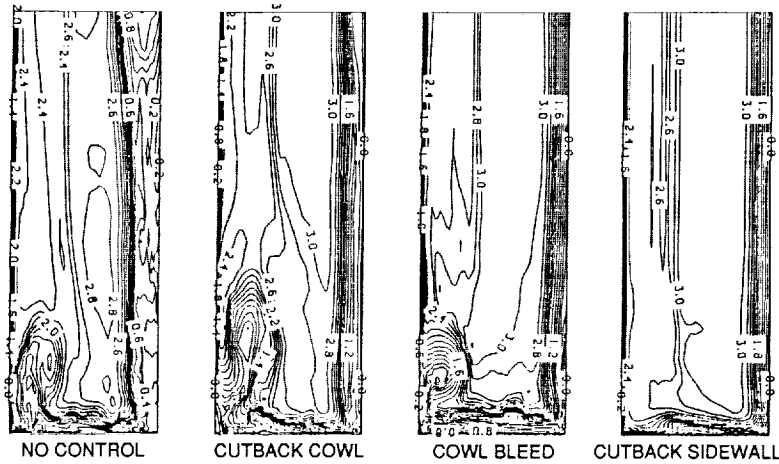


Figure 16. - Comparison of effect of various control methods on mach number contours near ramp shoulder (ref. 8).

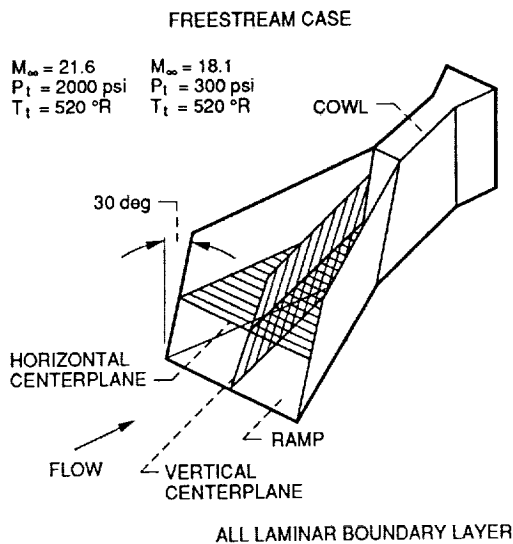


Figure 17. - Sidewall compression inlet schematic (ref. 9).

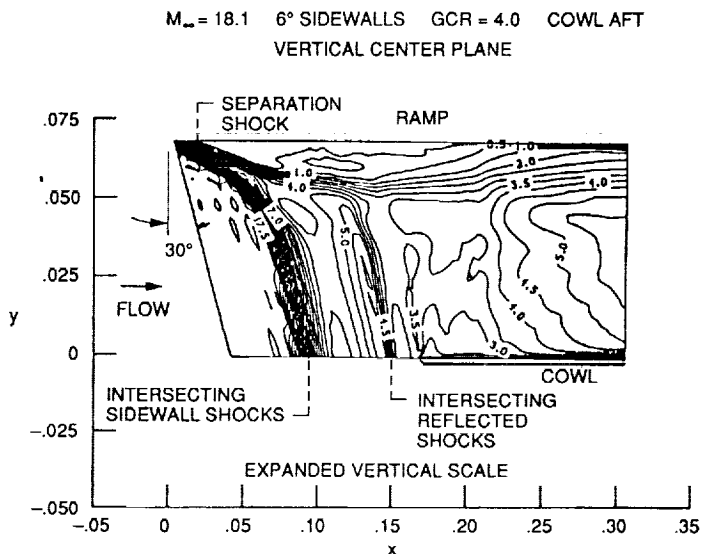


Figure 18. - Mach number contours for freestream case (ref. 9).

$M_\infty = 18.1$  6° SIDEWALLS GCR = 4.0 COWL AFT  
 HORIZONTAL CENTER PLANE  
 EXPANDED LATERAL SCALE

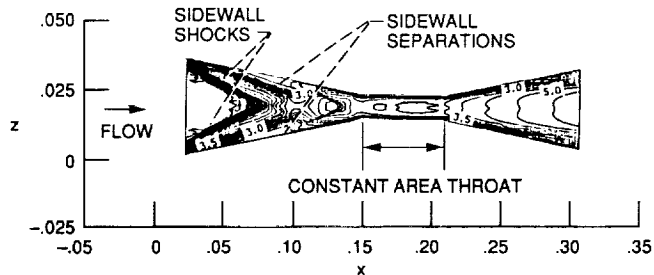


Figure 19. - Mach number contours for a representative freestream case in the horizontal center plane (ref. 9).

$M_\infty = 17.7$  6° SIDEWALLS GCR = 5.0 COWL AFT (100%)

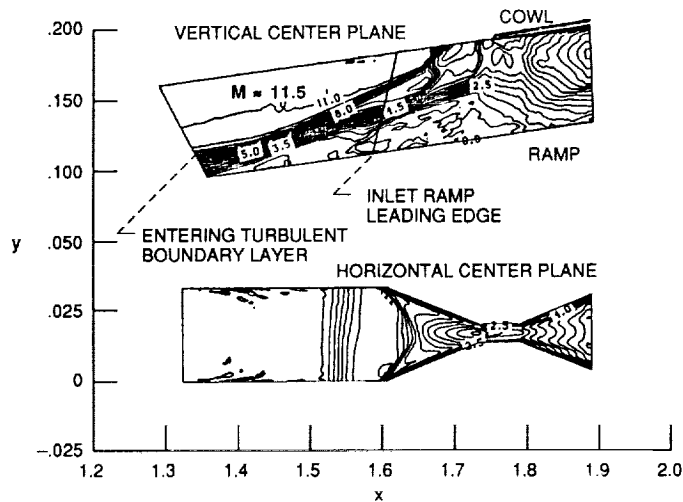


Figure 20. - Mach number contours for entering boundary layer case (ref. 9).

$M_\infty = 17.7$  6° SIDEWALLS GCR = 5.0 WEDGE CASE  
 RAMP CENTERLINE

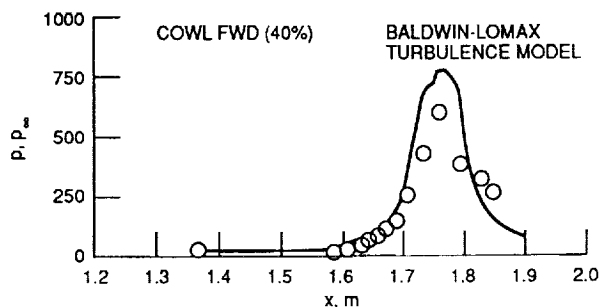


Figure 21. - Comparison of experimental and numerical surface pressure distributions (ref. 9).



# Report Documentation Page

|   |  |  |   |                            |                   |
|---|--|--|---|----------------------------|-------------------|
| 1. Report No.<br>NASA TM-103111   |  | 2. Government Accession No.                          |   | 3. Recipient's Catalog No. |                   |
| 4. Title and Subtitle<br>Computational Modeling and Validation for Hypersonic Inlets  |  |  | 5. Report Date  |                            |                   |
|   |  |  | 6. Performing Organization Code   |                            |                   |
| 7. Author(s)<br>Louis A. Povinelli  |  |  | 8. Performing Organization Report No.<br>E-5435   |                            |                   |
|   |  |  | 10. Work Unit No.<br>505-62-21  |                            |                   |
| 9. Performing Organization Name and Address<br>National Aeronautics and Space Administration<br>Lewis Research Center<br>Cleveland, Ohio 44135-3191   |  |  | 11. Contract or Grant No.   |                            |                   |
|   |  |  | 13. Type of Report and Period Covered<br>Technical Memorandum   |                            |                   |
| 12. Sponsoring Agency Name and Address<br>National Aeronautics and Space Administration<br>Washington, D.C. 20546-0001  |  |  | 14. Sponsoring Agency Code  |                            |                   |
|   |  |  | 15. Supplementary Notes<br>Prepared for the 75th Symposium on Hypersonic Combined Cycle Propulsion sponsored by the Propulsion and Energetics Panel of AGARD, Madrid, Spain, May 28-June 1, 1990. |                            |                   |
| 16. Abstract<br>Hypersonic inlet research activity at NASA is reviewed. The basis for the paper is the experimental tests performed with three inlets: the NASA Lewis Research Center Mach 5, the McDonnell Douglas Mach 12, and the NASA Langley Mach 18. Both three-dimensional PNS and NS codes have been used to compute the flow within the three inlets. Modeling assumptions in the codes involve the turbulence model, the nature of the boundary layer, shock wave-boundary layer interaction, and the flow spilled to the outside of the inlet. Use of the codes in conjunction with the experimental data are helping to develop a clearer understanding of the inlet flow physics and to focus on the modeling improvements required in order to arrive at validated codes. |  |  |   |                            |                   |
| 17. Key Words (Suggested by Author(s))<br>CFD<br>Hypersonic propulsion<br>Propulsion CFD<br>High speed inlets   |  |  | 18. Distribution Statement<br>Unclassified-Unlimited<br>Subject Category 34   |                            |                   |
| 19. Security Classif. (of this report)<br>Unclassified  |  | 20. Security Classif. (of this page)<br>Unclassified |   | 21. No. of pages<br>10     | 22. Price*<br>A03 |